On the Dispersion Errors Related to $(FD)^2TD$ Type Schemes

Jeffrey L. Young, *Member, IEEE*, Amorn Kittichartphayak, Yuk Ming Kwok, and Dennis Sullivan

***Abstract*— The dispersion errors associated with various frequency-dependent FDTD methods are considered herein. Particularly, we provide a rigorous error analysis of both direct integration and recursive type schemes for two media models: The one-pole Debye and the two-pole Lorentz. The error equations are cast in terms of a dispersion relation that shows explicitly the errors associated with numerically induced dispersion and dissipation. From the dispersion relation, plots are provided that typify the errors of each method. In general, all methods have about the same propagation characteristics; the differences, however, are seen in the attenuation plots. To validate the claims herein, data obtained from FDTD scattering simulations (both 1-D and 3-D geometries) are also given.**

I. Introduction

OVER THE PAST several years researchers have been extending the classic finite-difference time-domain (FDTD) method to handle frequency dependent media; the methods bear the acronym of $(FD)^2TD$, which is the extended acronym for frequency dependent FDTD. These new methods can be divided into two basic categories: The recursive convolution (RC) methods [1]–[4] and the direct integration (DI) methods [5]–[9]. The RC methods utilize the property that the time-domain constitutive relation between the displacement vector and the electric field vector is given as a convolution integral whose time-domain susceptibility function is known. Although the convolution operation implies the storage of the electric field's complete time history, a recursive summation can be derived that requires only the storage of a few previous values of the electric field; the actual number of previous values is dependent upon the number of poles in the frequency-domain susceptibility function.

In addition to Maxwell's equations, the DI methods consider an auxiliary set of differential equations. These equations can be obtained either by considering the frequency-domain constitutive polynomial as a differential equation in the time-domain [7], [8] or by considering the governing equations on which the constitutive relation is based [5], [6], [9].

In this paper we investigate in detail the RC methods proposed by Luebbers *et al.* [1], [3] (referred to as just Luebbers throughout the remainder of this manuscript) and the DI methods of Young [9]. These two methods are chosen since they require a minimal amount of computational memory, are postulated for any number of relaxations or resonances in the medium and invoke the principle of explicit time integration. In addition, we will also consider the method of Joseph *et al.* [7] (referred to as just Joseph throughout the remainder of this manuscript), due to the popularity of the method as well as the availability of error information [10]. (Other methods, such as those of Kashiwa *et al.* [5], [6] and the method of Sullivan [4], are not considered; the former was analyzed by Petropoulos [10] and the latter has many of the same properties as the RC methods of Luebbers.)

The main point of comparison is the numerical dispersion errors introduced by each of these schemes. For this reason, a rigorous error analysis is given with the final result cast in terms of a dispersion relationship of the form $\omega^2\epsilon_r = c^2k^2$, where ϵ_r is the relative permittivity of the medium. Due to the simplicity of the dispersion relationship, phase and attenuation errors can be readily deduced.

Two types of media are considered herein. The first is the single pole model of Debye, which is mathematically defined according the permittivity relation [11]

$$\epsilon_r = \epsilon_\infty + \frac{\epsilon_s - \epsilon_\infty}{1 + j\omega t_o}. \tag{1}$$

Here ϵ_∞ is the permittivity at infinite frequency and ϵ_s is the permittivity at DC; t_o is the relaxation time. The second is the Lorentzian two pole model; for this case

$$\epsilon_r = \epsilon_\infty + \frac{(\epsilon_s - \epsilon_\infty)\omega_1^2}{\omega_1^2 + j\omega\nu - \omega^2}. \tag{2}$$

In addition to ϵ_∞ and ϵ_s, ω_1 is the resonant frequency and ν is the damping coefficient.

II. Recursive Schemes

The time-domain constitutive relation between the displacement vector $\boldsymbol{D}$ and the electric field vector $\boldsymbol{E}$ forms the basis of the recursive type schemes. Assuming isotropic media, we write

$$\boldsymbol{D}(\boldsymbol{x}, t) = \epsilon_\infty\epsilon_o\boldsymbol{E}(\boldsymbol{x}, t) + \epsilon_o\int_0^t \boldsymbol{E}(\boldsymbol{x}, t-\tau)\chi(\tau)\, d\tau \tag{3}$$

where χ is the electric susceptibility. Under the assumption that $\boldsymbol{E}$ is piece-wise constant over the time interval δ_t, then $\boldsymbol{D}$ at time $t = n\delta_t$ is approximated by

$$\boldsymbol{D}(\boldsymbol{x}, n\delta_t) \approx \epsilon_\infty\epsilon_o\boldsymbol{E}(\boldsymbol{x}, n\delta_t) + \epsilon_o\sum_{m=0}^{n-1}\boldsymbol{E}(\boldsymbol{x}, (n-m)\delta_t)\chi^m \tag{4}$$

Manuscript received September 16, 1994; revised April 24, 1995. This work was supported in part by the NASA Space Engineering Research Center Contract NAGW-3293 and 3-26411-7800, the Idaho State Board of Education, and the University of Idaho Research Office.

The authors are with the NASA Space Engineering Research Center, Department of Electrical Engineering, University of Idaho, Moscow, ID 83844 USA.

IEEE Log Number 9412682.

with χ^m being defined as

$$\chi^m = \int_{m\delta_t}^{(m+1)\delta_t} \chi(\tau)\, d\tau. \tag{5}$$

Similarly, at time $t = (n+1)\delta_t$,

$$\boldsymbol{D}(\boldsymbol{x},(n+1)\delta_t) \approx \epsilon_\infty \epsilon_o \boldsymbol{E}(\boldsymbol{x},(n+1)\delta_t) + \epsilon_o \sum_{m=0}^{n} \boldsymbol{E}(\boldsymbol{x},(n-m+1)\delta_t)\chi^m. \tag{6}$$

Thus, upon the invocation of the central difference approximation for the time derivative, the displacement current at time $(n+1/2)\delta_t$ is deduced from (4) and (6), and is set to equal the curl of the magnetic field $\boldsymbol{H}$, per Ampere's law:

$$\epsilon_o\epsilon_\infty[\boldsymbol{E}(\boldsymbol{x},(n+1)\delta_t) - \boldsymbol{E}(\boldsymbol{x},n\delta_t)] + \epsilon_o \boldsymbol{E}(\boldsymbol{x},(n+1)\delta_t)\chi^0 - \epsilon_o \sum_{m=0}^{n-1} \boldsymbol{E}(\boldsymbol{x},(n-m)\delta_t)\Delta\chi^m \approx \delta_t \nabla \times \boldsymbol{H}(\boldsymbol{x},(n+1/2)\delta_t), \tag{7}$$

where

$$\Delta\chi^m = \chi^m - \chi^{m+1}. \tag{8}$$

Further arrangement of terms leads to an explicit equation for $\boldsymbol{E}$

$$\boldsymbol{E}(\boldsymbol{x},(n+1)\delta_t) = \left(\frac{1}{\epsilon_\infty + \chi^0}\right)(\epsilon_\infty \boldsymbol{E}(\boldsymbol{x},n\delta_t) + \sum_{m=0}^{n-1} \boldsymbol{E}(\boldsymbol{x},(n-m)\delta_t)\Delta\chi^m + (\delta_t/\epsilon_o)\nabla \times \boldsymbol{H}(\boldsymbol{x},(n+1/2)\delta_t)). \tag{9}$$

Provided that the susceptibility function can be cast in terms of an exponential, the summation in (9) can be replaced with a recursive or update type equation [1]–[3].

Using similar arguments as above and assuming nonmagnetized media, we note that the discretized form for Faraday's law is simply

$$\mu_o[\boldsymbol{H}(\boldsymbol{x},(n+1/2)\delta_t) - \boldsymbol{H}(\boldsymbol{x},(n-1/2)\delta_t)] \approx -\delta_t \nabla \times \boldsymbol{E}(\boldsymbol{x},n\delta_t). \tag{10}$$

Equations (9) and (10) are the temporally discretized RC field equations for dispersive media and are valid for any causal susceptibility function.

To consider the dispersion errors created by the aforementioned discretization scheme, assume that $\boldsymbol{E}(\boldsymbol{x},t) = \boldsymbol{e}(\boldsymbol{k},\omega)\exp(j\omega t - j\boldsymbol{k}\cdot\boldsymbol{x})$ and $\boldsymbol{H}(\boldsymbol{x},t) = \boldsymbol{h}(\boldsymbol{k},\omega)\exp(j\omega t - j\boldsymbol{k}\cdot\boldsymbol{x})$. Then in Yee space, (9) and (10) reduce to

$$j\Omega\epsilon_r\epsilon_o\boldsymbol{e}(\boldsymbol{k},\omega) = -j\boldsymbol{K}\times\boldsymbol{h}(\boldsymbol{k},\omega) \tag{11}$$

and

$$j\Omega\mu_o\boldsymbol{h}(\boldsymbol{k},\omega) = j\boldsymbol{K}\times\boldsymbol{e}(\boldsymbol{k},\omega) \tag{12}$$

where

$$\Omega = \frac{2}{\delta_t}\sin\left(\frac{\omega\delta_t}{2}\right) \tag{13}$$

and

$$\boldsymbol{K} = \frac{2}{\delta_x}\sin\left(\frac{k_x\delta_x}{2}\right)\boldsymbol{a_x} + \frac{2}{\delta_y}\sin\left(\frac{k_y\delta_y}{2}\right)\boldsymbol{a_y} + \frac{2}{\delta_z}\sin\left(\frac{k_z\delta_z}{2}\right)\boldsymbol{a_z}. \tag{14}$$

Here δ_x, δ_y and δ_z are the cell dimensions and k_x, k_y and k_z are the components of the wavenumber $\boldsymbol{k}$. As expected, $\boldsymbol{K} \to \boldsymbol{k}$ and $\Omega \to \omega$ as $\delta_{x,y,z} \to 0$ and $\delta_t \to 0$, respectively. Also

$$\epsilon_r = \epsilon_\infty + \frac{\chi^0 e^{j\omega\delta_t/2} - Se^{-j\omega\delta_t/2}}{j\Omega\delta_t} \tag{15}$$

which is the numerical permittivity function and

$$S = \sum_{m=0}^{n-1} e^{-j\omega m\delta_t}\Delta\chi^m \tag{16}$$

which is the medium's memory function. After further vector manipulation, the dispersion relation is deduced from (11) and (12) and is found to be

$$\epsilon_r\Omega^2 = c^2\boldsymbol{K}\cdot\boldsymbol{K}. \tag{17}$$

Note: Except for the presence of ϵ_r, the previous numerical dispersion relation is the numerical dispersion relation for free-space propagation [12].

A. Debye Medium

Consider the case when the medium is ascribed by the name of Debye. Whence [1]

$$\chi(t) = \frac{(\epsilon_s - \epsilon_\infty)}{t_o}e^{-t/t_o}u(t), \tag{18}$$

$$\chi^m = (\epsilon_s - \epsilon_\infty)(1 - e^{-\delta_t/t_o})e^{-m\delta_t/t_o} \tag{19}$$

and

$$\Delta\chi^m = (\epsilon_s - \epsilon_\infty)(1 - e^{-\delta_t/t_o})^2 e^{-m\delta_t/t_o}. \tag{20}$$

Then by inserting the previous relation into (16), we obtain

$$S = (\epsilon_s - \epsilon_\infty)(1 - e^{-\delta_t/t_o})^2 \sum_{m=0}^{n-1} z^m = (\epsilon_s - \epsilon_\infty)(1 - e^{-\delta_t/t_o})^2\left(\frac{1-z^n}{1-z}\right) \tag{21}$$

where

$$z = e^{-(\delta_t/t_o)(1+j\omega t_o)}. \tag{22}$$

By definition, steady-state is reached when $n \to \infty$. Since z^n exponentially decays as n is increased, we conclude that

$$S = (\epsilon_s - \epsilon_\infty)(1 - e^{-\delta_t/t_o})^2\left(\frac{1}{1-z}\right) \tag{23}$$

or explicitly,

$$S = \frac{(\epsilon_s - \epsilon_\infty)(1 - e^{-\delta_t/t_o})^2 e^{(\delta_t/t_o)(1+j\omega t_o)/2}}{2\sinh[(\delta_t/t_o)(1+j\omega t_o)/2]}. \tag{24}$$

Therefore, for a Debye medium and from (15) and (24), the numerical permittivity is given by

$$\epsilon_r = \epsilon_\infty + \frac{\chi^0 e^{j\omega\delta_t/2}}{j\Omega\delta_t} - \frac{(\epsilon_s - \epsilon_\infty)(1 - e^{-\delta_t/t_o})^2 e^{\delta_t/(2t_o)}}{2j\Omega\delta_t \sinh[(\delta_t/t_o)(1 + j\omega t_o)/2]}. \quad (25)$$

It can be argued from the numerator of (25) that this RC scheme is only first order accurate in time, since for small δ_t $\exp[j\omega\delta_t/2] \approx 1 + j\omega\delta_t/2$. This is to be expected since the electric field is assumed to be piece-wise constant over each time step in the evaluation of the convolution integral. Also, if δ_t is allowed to become infinitesimally small, (25) reduces to the exact answer given by (1).

To prove this last point, first let δ_t/t_o become vanishingly small. Then, recognizing that

$$\sinh[(\delta_t/t_o)(1 + j\omega t_o)/2] \approx \left(\frac{\delta_t}{2t_o}\right)(\Lambda + j\Omega t_o) \quad (26)$$

we can write (25) as follows:

$$\epsilon_r \approx \epsilon_\infty + \frac{(\epsilon_s - \epsilon_\infty)e^{j\omega\delta_t/2}}{j\Omega t_o} - \frac{\epsilon_s - \epsilon_\infty}{j\Omega t_o(\Lambda + j\Omega t_o)}. \quad (27)$$

In the previous expressions, $\Lambda = \cos(\omega\delta_t/2)$. Now if $\omega\delta_t \to 0$, then $\Lambda \to 1, \Omega \to \omega$ and (27) reduces to (1).

B. Lorentz Medium

The derivation for the two-pole Lorentz medium is similar to the one given above. To begin with, the time-domain susceptibility function under consideration is [3]

$$\chi(t) = \gamma e^{-\alpha t} \sin(\beta t)u(t) \quad (28)$$

where $\beta = \sqrt{\omega_1^2 - \alpha^2}, \alpha = \nu/2$ and $\gamma\beta = \omega_1^2(\epsilon_s - \epsilon_\infty)$. When the summation S is evaluated and n is allowed to approach infinity, it is found that $S = S_1 + S_2$, where

$$S_1 = \frac{-Ae^{-j(\beta - \omega + j\alpha)\delta_t/2}}{4j \sin[(\beta - \omega + j\alpha)\delta_t/2]} \quad (29)$$

and

$$S_2 = \frac{-A^* e^{-j(-\beta - \omega + j\alpha)\delta_t/2}}{4j \sin[(-\beta - \omega + j\alpha)\delta_t/2]} \quad (30)$$

where the asterisk denotes the complex conjugate; also

$$A = \left(\frac{-j\gamma}{\alpha - j\beta}\right)(1 - e^{(-\alpha + j\beta)\delta_t})^2. \quad (31)$$

(Note: For low loss situations, S_1 captures the resonant effect, for frequencies very near the resonant frequency.) The numerical permittivity relation is obtained when the expression $S_1 + S_2$ is inserted into (15)

$$\epsilon_r = \epsilon_\infty + \frac{\chi^0 e^{j\omega\delta_t/2} - (S_1 + S_2)e^{-j\omega\delta_t/2}}{j\Omega\delta_t} \quad (32)$$

where, for the Lorentz media

$$\chi^0 = \mathrm{Re}\left\{\frac{-j\gamma}{\alpha - j\beta}(1 - e^{(-\alpha + j\beta)\delta_t})\right\}. \quad (33)$$

Again, the first order accuracy is manifested in (32). Even so, as δ_t becomes small, the permittivity relation converges to the exact answer given by (2).

Now consider the case when $\beta\delta_t \ll 1$ and $\alpha\delta_t \ll 1$. For this situation

$$S \approx \frac{-j\beta\gamma\Omega\delta_t e^{j\omega\delta_t/2}}{(\beta^2 + \alpha^2)\Lambda^2 + 2j\alpha\Lambda\Omega - \Omega^2}. \quad (34)$$

Upon the insertion of (34) into (32) and the substitution of parameters, one obtains

$$\epsilon_r \approx \epsilon_\infty + \frac{\omega_1^2(\epsilon_s - \epsilon_\infty)}{\omega_1^2\Lambda^2 + j\nu\Lambda\Omega - \Omega^2} \quad (35)$$

which bears some resemblance to (2).

III. Direct Integration Schemes

A. Debye Medium

For the Debye medium, the direct integration scheme given by Young is founded on the following differential equations [5], [9]:

$$\epsilon_o\epsilon_\infty \frac{\partial \boldsymbol{E}}{\partial t} = \nabla \times \boldsymbol{H} - \frac{1}{t_o}[(\epsilon_s - \epsilon_\infty)\epsilon_o \boldsymbol{E} - \boldsymbol{P}], \quad (36)$$

$$\mu_o \frac{\partial \boldsymbol{H}}{\partial t} = -\nabla \times \boldsymbol{E} \quad (37)$$

and

$$\frac{d\boldsymbol{P}}{dt} = \frac{1}{t_o}[(\epsilon_s - \epsilon_\infty)\epsilon_o \boldsymbol{E} - \boldsymbol{P}] \quad (38)$$

where $\boldsymbol{P}$ is the polarization vector. To accomplish the temporal discretization, central differences are used for each of the time derivatives; where two like quantities appear in the left and right hand sides of the same equation, central averages are invoked. The equations are advanced in time according to the leap-frog strategy. That is, (37) and (38) are advanced simultaneously and leaped with (36).

The error analysis that was presented for the RC methods is duplicated here. Suppressing the algebraic steps, we find that the numerical permittivity is given by the following equation:

$$\epsilon_r = \epsilon_\infty + (\epsilon_s - \epsilon_\infty)\left[\frac{\Lambda + j(\delta_t/2)^2(\Omega/t_o)}{\Lambda + jt_o\Omega}\right]. \quad (39)$$

Obviously, as δ_t becomes vanishingly small, the numerical permittivity reduces to the exact expression; the rate of convergence is second order. Even so, for a non-zero time step, we see that the effective relaxation time t_o' is frequency dependent and is given by $t_o' = t_o\Psi/\Lambda$, where $\Psi = \Omega/\omega$; similarly, the effective permittivity difference $\epsilon_s - \epsilon_\infty$ is complex and frequency dependent. For accurate solutions, we see that it is desirable to keep Ψ/Λ as close to unity and $(\delta_t/2)^2(\Omega/t_o)$ close to zero as possible for all frequencies of interest.

In addition to Ampere's and Faraday's laws, Joseph [7] considered the following time-domain constitutive relation

$$t_o\epsilon_\infty\epsilon_o \frac{d\boldsymbol{E}}{dt} = -\epsilon_s\epsilon_o \boldsymbol{E} + \boldsymbol{D} + t_o \frac{d\boldsymbol{D}}{dt}. \quad (40)$$

Again, central differences and averages are used to discretize the above equation, where appropriate, and an explicit expression for $\boldsymbol{E}$ is deduced from past values of $\boldsymbol{E}$, and current and past values of $\boldsymbol{D}$. With respect to the numerical permittivity, Petropoulos [10] has shown that

$$\epsilon_r = \epsilon_\infty + (\epsilon_s - \epsilon_\infty)\left[\frac{\Lambda}{\Lambda + jt_o\Omega}\right]. \tag{41}$$

Comparing (39) with (41), we conclude that the method of Joseph is more accurate than the method of Young, due to the additional term $j(\delta_t/2)^2(\Omega/t_o)$ that shows up in (39). However, both DI schemes will result in identical effective relaxation times.

B. Lorentz Medium

We now turn our attention to Young's DI scheme in association with the Lorentz medium. To begin with, the appropriate differential equations are presented below [6], [9]:

$$\epsilon_o\epsilon_\infty\frac{\partial \boldsymbol{E}}{\partial t} = \nabla \times \boldsymbol{H} - \boldsymbol{J}_p, \tag{42}$$

$$\mu_o\frac{\partial \boldsymbol{H}}{\partial t} = -\nabla \times \boldsymbol{E}, \tag{43}$$

$$\frac{d\boldsymbol{J}_p}{dt} = -\nu\boldsymbol{J}_p + (\epsilon_s - \epsilon_\infty)\epsilon_o\omega_1^2\boldsymbol{E} - \omega_1^2\boldsymbol{P}, \tag{44}$$

and

$$\frac{d\boldsymbol{P}}{dt} = \boldsymbol{J}_p \tag{45}$$

where, in addition to the symbols defined earlier, the polarization current $\boldsymbol{J}_p$ has also been introduced. Again, the temporal discretization is accomplished by using both central difference and average approximations, where appropriate. With respect to the leap-frog time advancement, (42) and (45) are advanced simultaneously and leaped with the simultaneous advancement of (43) and (44).

Regarding the numerical permittivity, it is easy to show that

$$\epsilon_r = \epsilon_\infty + \frac{(\epsilon_s - \epsilon_\infty)\omega_1^2}{\omega_1^2 + j\nu\Omega\Lambda - \Omega^2}. \tag{46}$$

Again we note that the exact expression is obtained when δ_t approaches zero. For non-zero δ_t, it is appropriate to define an effective, frequency-dependent resonant frequency ω_1' and damping frequency ν'. For the case at hand, it is seen that $\omega_1' = \omega_1/\Psi$ and $\nu' = \nu\Lambda/\Psi$. For Lorentz media, accurate solutions are obtained when both Ψ and Λ/Ψ are near unity.

A few other observations are in order. First, the DI and the RC methods yield similar results, as manifested by (35) and (46), when $\beta\delta_t$ and $\alpha\delta_t$ tend to zero. Second, when the media is dissipationless (i.e., $\nu = 0$), we observe that this DI scheme is also dissipationless; this is not the case for the RC scheme of Luebbers.

Due to the simplicity of (46), we can ascertain the stability of Young's scheme rather readily by considering the dispersion relationship defined by (17) and by setting ν to a value of zero. The solution, in terms of Ω, is found to be

$$\Omega^2 = \kappa_1 + \sqrt{\kappa_1^2 - \kappa_2} \tag{47}$$

where

$$\kappa_1 = \frac{\epsilon_s\omega_1^2 + c^2\boldsymbol{K}\cdot\boldsymbol{K}}{2\epsilon_\infty} \tag{48}$$

and

$$\kappa_2 = \frac{c^2\omega_1^2\boldsymbol{K}\cdot\boldsymbol{K}}{\epsilon_\infty}. \tag{49}$$

By definition, Ω is the eigenvalue associated with central difference approximation of the continuous operator $\partial/\partial t$. Thus, if

$$\frac{\partial \boldsymbol{v}}{\partial t} = \boldsymbol{L}\boldsymbol{v} \tag{50}$$

represents the system of partial differential equations to be solved, where $\boldsymbol{L}$ is the spatial operator and $\boldsymbol{v}$ is the unknown, then the square root of the right hand side (47) is the numerical eigenvalue of $\boldsymbol{L}$. Stability requires that the imaginary part of the eigenvalue be less than $2/\delta_t$ [13]. Hence, for all propagating modes, stability is insured if

$$\kappa_3 + \sqrt{\kappa_3^2 - \kappa_4} \le \left(\frac{2}{h}\right)^2. \tag{51}$$

For one-dimensional propagation

$$\kappa_3 = \frac{\epsilon_s\omega_1^2 + c^2(2/\delta_x)^2}{2\epsilon_\infty} \tag{52}$$

and

$$\kappa_4 = \frac{c^2\omega_1^2(2/\delta_x)^2}{\epsilon_\infty}. \tag{53}$$

With respect to the method of Joseph [7], the following time-domain constitutive relation is considered in conjunction with the curl equations of Maxwell

$$\epsilon_\infty\epsilon_o\frac{d^2\boldsymbol{E}}{dt^2} = -\nu\epsilon_\infty\epsilon_o\frac{d\boldsymbol{E}}{dt} - \omega_1^2\epsilon_s\epsilon_o\boldsymbol{E} + \omega_1^2\boldsymbol{D} + \nu\frac{d\boldsymbol{D}}{dt} + \frac{d^2\boldsymbol{D}}{dt^2}. \tag{54}$$

Again, the discretization is accomplished by using central differences and averages. From this, it can be shown that [10]

$$\epsilon_r = \epsilon_\infty + \frac{(\epsilon_s - \epsilon_\infty)\omega_1^2\cos(\omega\delta_t)}{\omega_1^2\cos(\omega\delta_t) + j\nu\Omega\Lambda - \Omega^2}. \tag{55}$$

Upon the comparison of (46) with (55), it is seen that Young's and Joseph's method yield nearly identical results. Note: The effective resonant frequencies are different whereas the damping frequencies are the same. In the case of Joseph's method, $\omega_1' = \omega_1\sqrt{\cos(\omega\delta_t)}/\Psi$. Finally, for lossless media, the scheme of Joseph is also dissipationless. (For a stability analysis, see [10].)

IV. FDTD Parameters

Now that each of the schemes have been analytically characterized, it is important to state the general procedure for setting the parameters δ_t and $\delta_{r,y,z}$. First, the spatial step is selected according to the rule that the propagating wave be sampled N times per wavelength, λ_o. For example,

$$\delta_x = \frac{\lambda_o}{N} = \frac{v_o}{N f_o} \tag{56}$$

where v_o is the corresponding phase velocity at the frequency f_o (i.e., $v_o = v|_{f=f_o}$). The time step is then deduced from a stability formula, such as (51) or those given in [10]. (In the absence of a media dependent criterion, one can try the relation $\delta_t = \delta_x/(2v_{\max})$, where $v_{\max}$ is the maximum phase velocity.)

Once δ_t and δ_x are specified, (17) is used to deduce the numerical wave number. For example, in a one-dimensional space, k (as a function of ω, δ_t and δ_x) is easily determined from (17)

$$k = \left(\frac{2}{\delta_x}\right) \sin^{-1}\left[\frac{\delta_x\sqrt{\epsilon_r}}{\delta_t c}\sin\left(\frac{\omega\delta_t}{2}\right)\right]. \tag{57}$$

Dispersion and attenuation surfaces can now be plotted using (57) and compared with that obtained from the exact answer: $c^2k^2 = \epsilon_r\omega^2$. If the comparison is not favorable, then the parameter N should be adjusted until the error (i.e., the difference of the two surfaces) is an acceptable value at f_o. The total error accumulation is computed by multiplying the error by the total distance the wave will travel during an elapsed time of $M\delta_t$ [14], where M is the number of time steps.

V. Numerical Results

To bring to light the various dispersion errors introduced by the aforementioned schemes, it is advantageous to consider and plot the following relative error functions

$$e^{\text{real}} = \left|\frac{\text{Re}\{k - k^{\text{fdtd}}\}}{\text{Re}\{k\}}\right| \tag{58}$$

and

$$e^{\text{imag}} = \left|\frac{\text{Im}\{k - k^{\text{fdtd}}\}}{\text{Im}\{k\}}\right| \tag{59}$$

where k^{fdtd} is a solution of (57) and k is a solution of $\omega^2\epsilon_r = c^2k^2$. Under the assumption that the waves are of the form $\exp[-jkx + j\omega t]$, it is apparent that e^{real} is a measure of the numerical phase error and e^{imag} is a measure of the numerical attenuation error.

First consider the Debye model for water, which is characterized by the following parameters: $\epsilon_s = 81, \epsilon_\infty = 1.8$ and $t_o = 9.4$ ps; for the FDTD parameters, let $h_x = 37.5\,\mu$m and $\delta_t = 62.5$ fs [1]. Figs. 1 and 2 show the logarithm of the error metrics, as defined by (58) and (59), respectively. With respect to the phase errors, it is apparent from Fig. 1 that for a given allowance of phase error, the DI schemes have more bandwidth than the RC scheme. Also of interest are the flat dissipation errors for the RC scheme and the DI scheme of Young, as seen from Fig. 2. Although the dissipation errors are higher at lower

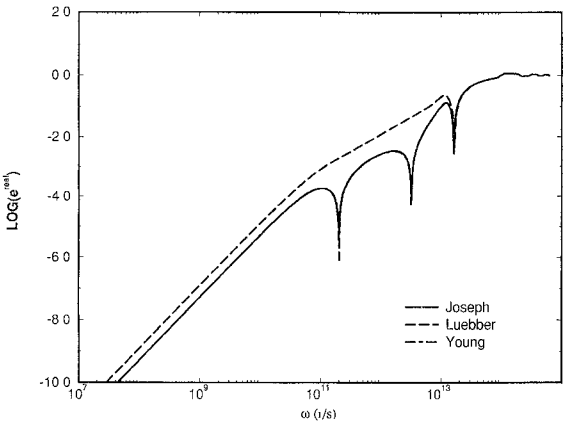

Fig. 1. The logarithm of the phase error as a function of frequency: Debye media.

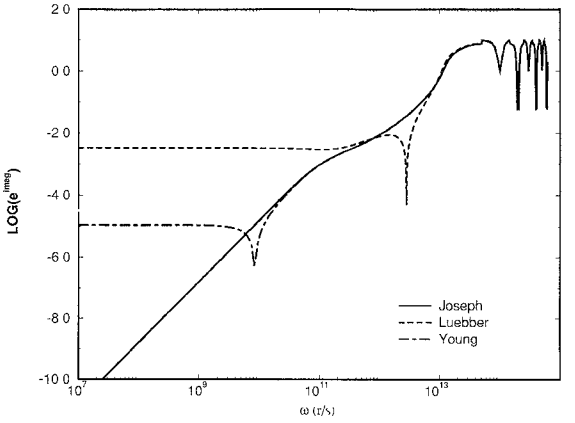

Fig. 2. The logarithm of the attenuation error as a function of frequency: Debye media.

frequencies, we see that the RC scheme can possibly achieve more bandwidth, from a dissipation type criteria. Finally, in the high frequency limit, observe from Figs. 1 and 2 that all three schemes converge to about the same error values.

Using these same parameters, we now consider a one-dimensional FDTD simulation of a plane wave scattering from a Debye slab; the chosen field components are E_x and H_y. The computational domain consists of a 1500 cells, 375 of which span the slab. Assuming an incident Gaussian pulsed plane wave of the form $\exp((t - (x - x_o)/c)^2w^2)$, where $w = 1.64 \times 10^{11}$ s^{-1} and $x_o = 450\,\delta_x$, and allowing the clock to run for 1500 time steps, we obtained the results plotted in Fig. 3 for all three methods. (Note that this choice of w realizes an input pulse that has a usable frequency spectrum of about 80 GHz.) Since the relative differences of each method are not visible from Fig. 3, we also provide Table I, which tabulates the maximum and minimum values of the electric field as computed from the FDTD simulations and from the exact Fourier integral; the number in parenthesis is the relative error. (See Appendix A for more information on how the exact value is obtained.) As expected from the error plots of Figs. 1 and 2, Table I confirms that the overall accuracy of each method is excellent.

For the Lorentz media, let $\epsilon_s = 3, \epsilon_\infty = 1.5, \omega_1 = 2\pi \times 50 \times 10^9$ r/s, and $\nu = .2\omega_1, \delta_x = 37.5\,\mu$m and $\delta_t = 62.5$

TABLE I
THE COMPUTED ELECTRIC FIELD VALUES (V/m) FOR THE METHODS OF YOUNG, JOSEPH AND LUEBBERS: DEBYE SLAB THE RELATIVE ERROR IS PROVIDED IN PARENTHESIS

CELL #	YOUNG	JOSEPH	LUEBBERS	EXACT
304	-.7578 (.11%)	-.7578 (11%)	-.7575 (.15%)	-.7586
808	.03798 (.16%)	03798 (16%)	03806 (- 05%)	.03804

TABLE II
THE COMPUTED ELECTRIC FIELD VALUES (V/m) FOR THE METHODS OF YOUNG, JOSEPH AND LUEBBERS: LORENTZ SLAB THE RELATIVE ERROR IS PROVIDED IN PARENTHESIS

CELL #	YOUNG	JOSEPH	LUEBBERS	EXACT
317	-.3184 (0.00%)	-.3183 (0.03%)	-.3183 (0.03%)	-.3184
402	.1098 (-.18%)	.1098 (-.18%)	.1089 (.64%)	.1096
468	-.07333 (-.14%)	-.07336 (-.18%)	-.07243 (1.09%)	-.07323
534	.04387 (-.09%)	.04392 (-.21%)	.04312 (1.62%)	.04383
600	-.02303 (0.00%)	-.02308 (-.22%)	-.02252 (2.21%)	-.02303
667	.009746 (.13%)	.009766 (-.07%)	.009491 (2.75%)	.009759
734	-.002265 (.79%)	-.002274 (.39%)	-.002208 (3.29%)	-.002283
772	.01083 (-0.09%)	.01088 (-.55%)	.01056 (2.40%)	.01082
802	-.01147 (.69%)	-.01142 (1.13%)	-.01229 (6.41%)	-.01155
842	.04121 (-.51%)	.04138 (-.93%)	.04152 (-1.27%)	.04100
895	-.1030 (.10%)	-.1029 (.19%)	-.1035 (-.39%)	-.1031
985	.3709 (-.03%)	.3709 (-.03%)	.3728 (-.54%)	.3708

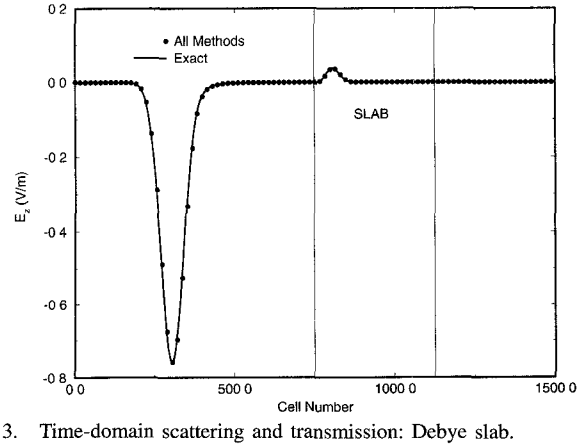

Fig. 3. Time-domain scattering and transmission: Debye slab.

fs [3]. Figs. 4 and 5 show the relative phase and attenuation errors, respectively. Again, the phase errors associated with each method are about the same. This is not the case with respect to the attenuation errors, where we observe that the RC scheme has about a flat five percent relative error. Even with high attenuation errors, the RC scheme gave satisfactory results in a one-dimensional FDTD simulation, as shown in Fig. 6. (In addition to the parameters listed above, we chose again a computational domain of 1500 cells and a running time of 1500 δ_t; we also assumed that $w = 1.64 \times 10^{11}$ s^{-1} and $x_o = 450\ \delta_x$.) However, after closer examination of data, it was found that the data associated with the RC scheme was not as accurate as the data associated with the two DI schemes. Particularly, we learn from Table II that the RC scheme has relative errors up to 6.41%, whereas the two RC schemes have relative errors no higher than 1.13%. It is surmized that the higher errors in the RC scheme are due to the high dissipation errors that are predicted by Fig. 5.

Finally, to conclude this section, consider the case of a plane wave scattered by a sphere comprised of a Lorentzian dielectric, whose dielectric parameters are the same as the aforementioned slab. The computational domain is a 50 cell cube and the diameter of the sphere is 20 cells. As far as the FDTD parameters are concerned, let $\delta_x = 37.5\,\mu$m and $\delta_t = 62.5$ fs, as before. Instead of time domain data, Figs. 7 and 8 show the frequency domain data for the impulse response of $|e_x(\omega, \boldsymbol{x})|$, as measured parallel to the x-axis and through the center of the sphere. Particularly, Fig. 7 is associated with the spectral frequences of 25 GHz, 50 GHz, and 100 GHz; whereas, Fig. 8 is for the spectral components at 200 and 400 GHz. (Note: In both figures only the data from one of the FDTD methods is shown due to the very close agreement between the data derived from each of the methods.) As seen from Figs. 7 and 8, the agreement between the FDTD results

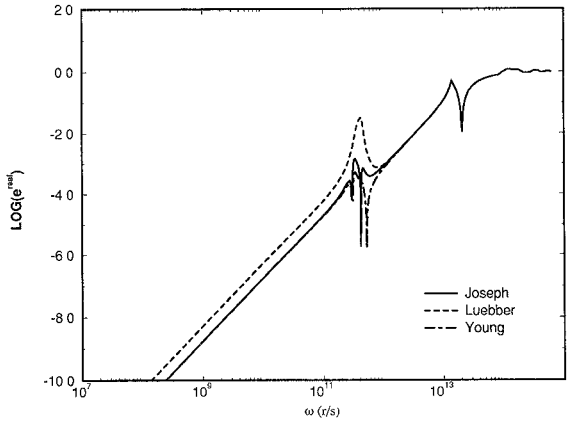

Fig. 4. The logarithm of the phase error as a function of frequency: Lorentz media.

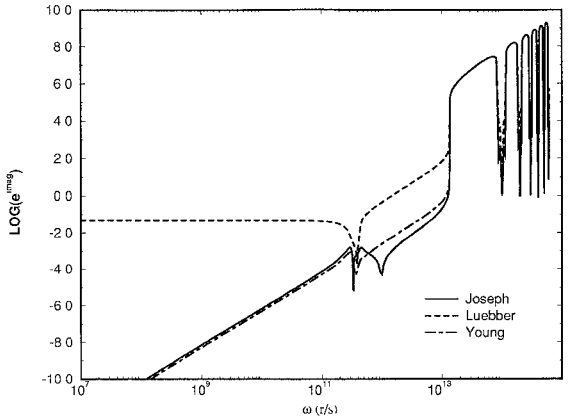

Fig. 5. The logarithm of the attenuation error as a function of frequency: Lorentz media.

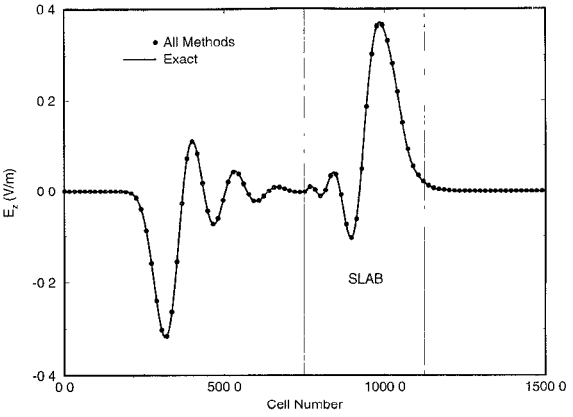

Fig. 6. Time-domain scattering and transmission. Lorentzian slab.

and the results obtained from the closed-form Mie solution [15] is fairly good. When the frequency was increased to 600 GHz, we observed no correlation between computed and exact. However, it was observed that the relative errors between all three FDTD methods were only about 1%. Even though the dispersion curves of Figs. 4 and 5 predict relatively low errors even at 600 GHz, we surmise that the disagreement is due more to boundary condition errors [16] rather than phase and attenuation related errors.

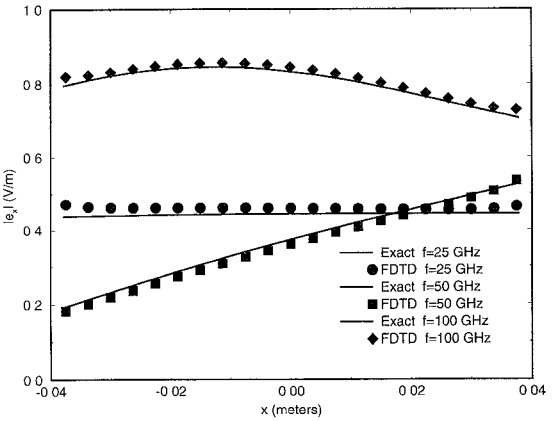

Fig. 7. Frequency-domain scattering from a Lorentzian sphere: $f = 25$, 50 and 100 GHz.

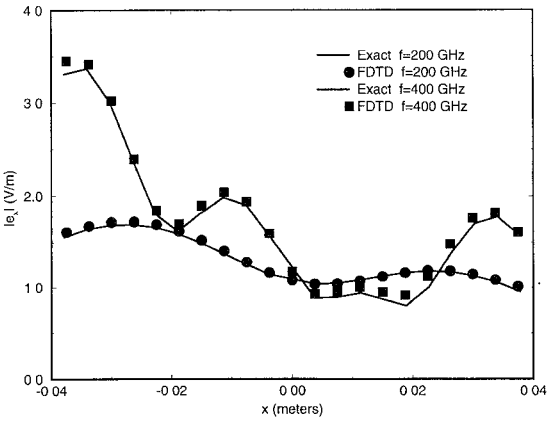

Fig. 8. Frequency-domain scattering from a Lorentzian sphere: $f = 200$ and 400 GHz.

VI. Conclusion

In this paper, three $(FD)^2TD$ type algorithms have been considered and studied in detail. After exhaustive simulations, we found that all three algorithms gave reasonably good results for typical choices of parameters, relaxations and resonances. Moreover, all schemes have about the same CPU burden (i.e., number of multiplications, additions, etc.), have the necessary simplicity (from a coding perspective) and introduce a certain amount of non-physical dispersion and/or dissipation into the numerical solution. When applied to three-dimensional problems, it was consistently observed that all three methods succeeded or failed in capturing the physical phenomena. More importantly, we surmise that other error sources, such as those associated with the stair-step modeling of a curve surface or an inhomogeneous medium, dominate errors due to artificial dispersion or dissipation. However, each algorithm does have its own peculiarities, deficiencies and strengths, as detailed next.

Except for a few cases, we were always able to get good results from the method of Joseph. This is to be expected since the truncation errors are all second order. For the cases when the method did give poor results (usually a result of setting the FDTD discretization parameters too coarse) it was found that the other two methods failed in the exact same way. Unfortunately, this method is memory expensive and is not

easily extended to account for media with multiple relaxations or resonances.

With respect to the method of Luebbers, the memory requirements are minimal (i.e., one additional memory cell per pole in the permittivity relation) and the adaptability of the algorithm to account for multiple relaxations or resonances is straight forward. The major shortcoming, however, is the first order nature of the convolution approximation. As the dispersion curves suggest, the phase characteristics are adequate but the attenuation characteristics can be poor. For late time investigations, the accumulation of attenuation errors may be too great for the RC simulation to yield accurate data.

Finally, Young's method is also second order accurate, memory parsimonious and flexible. For Debye media, the attenuation errors are typically poorer than those associated with the method of Joseph but usually better than those associated with the method of Luebbers. Also, for Lorentzian media, we found another deficiency: If the incident wave has all of its primary frequency content well below the resonant frequency (i.e., $\epsilon_r \approx \epsilon_s$) then the stability criterion requires too small of a time step for the algorithm to be of any practical value. Other than this case, the data derived from both DI simulations were virtually identical.

In conclusion, we feel that no one method can be labeled superior over the others. By carefully selecting the FDTD parameters, we were able to get superior or inferior results from all three methods. However, by using the error information provided herein, one can obtain readily dispersion curves that detail dispersion error information for the application at hand. From this, the time step and cell size can be chosen so that the user can apply each one of these algorithms with confidence.

APPENDIX A

The computed "exact" answer is obtained by numerically integrating the integral

$$\boldsymbol{e}(z,t) = \int_{-\infty}^{\infty} A(\omega)\boldsymbol{E}(z,\omega)e^{j\omega t}\, d\omega \tag{60}$$

where $\boldsymbol{E}(z,\omega)$ is the exact frequency domain solution [17] and $A(\omega)$ is the Fourier transform of the input pulse. Since the integrand decays like $e^{-\omega^2/(4w^2)}$ and $\boldsymbol{e}(z,t)$ is a real function, the above integral is well approximated by

$$\boldsymbol{e}(z,t) = 2\mathrm{Re}\left\{\int_0^a A(\omega)\boldsymbol{E}(z,\omega)e^{j\omega t}\, d\omega\right\} \tag{61}$$

where a is chosen such that $e^{-a^2/(4w^2)} = 10^{-16}$. Four point Gaussian quadrature is then applied over a span of $\Delta\omega$, which is determined initially from the zeros of the integrand, and the results of each sub-integration are summed to form the answer. To check accuracy, the integration span is halved and the integration is repeated; the new answer is compared with the old one. This process is repeated until the required accuracy is achieved. Certainly, more efficient procedures are available to accomplish the numerical integration (e.g. FFT) However, our ultimate concern for this investigation is accuracy, which is guaranteed by using this methodology.

ACKNOWLEDGMENT

The authors would like to express their gratitude to the anonymous reviewers for their valuable comments and suggestions.

REFERENCES

[1] R. Luebbers, F. P. Hunsberger, K. S. Kunz, R. B. Standler, and M. Schneider, "A frequency-dependent finite-difference time-domain formulation for dispersive materials," *IEEE Trans. Electromagn. Compat.*, vol. 32, pp. 222–227, 1990.

[2] R. J. Luebbers, F. Hunsberger, and K. S. Kunz, "A frequency-dependent finite-difference time-domain formulation for transient propagation in plasma," *IEEE Trans. Antennas Propagat.*, vol. 39, pp. 29–34, 1991.

[3] R. J. Luebbers and F. Hunsberger, "FDTD for Nth-order dispersive media," *IEEE Trans. Antennas Propagat.*, vol. 40, pp. 1297–1301, 1992.

[4] D. M. Sullivan, "Frequency-dependent FDTD methods using Z transforms," *IEEE Trans. Antennas Propagat.*, vol. 40, pp. 1223–1230, 1992.

[5] T. Kashiwa, N. Yoshida, and I. Fukai, "A treatment by the finite-difference time-domain method of the dispersive characteristics associated with orientation polarization," *IEICE Transactions*, vol. E–73, pp. 1326–1328, 1990.

[6] T. Kashiwa and I. Fukai, "A treatment by the FD-TD method of the dispersive characteristics associated with electronic polarization," *Microwave Opt. Tech. Lett.*, vol. 3, pp. 203–205, 1990.

[7] R. M. Joseph, S. C. Hagness, and A. Taflove, "Direct time integration of Maxwell's equations in linear dispersive media with absorption for scattering and propagation of femtosecond electromagnetic pulses," *Opt. Lett.*, vol. 16, pp. 1412–1414, 1991.

[8] O. P. Gandhi, B.-Q. Gao, and J.-Y. Chen, "A frequency-dependent finite-difference time-domain formulation for general dispersive media," *IEEE Trans. Microwave Theory Tech.*, vol. 41, pp. 658–665, 1993.

[9] J. L. Young, "Propagation in linear dispersive media: Finite difference time-domain methodologies," *IEEE Trans. Antennas Propagat.*, vol. 43, pp. 422–426, 1995.

[10] P. G. Petropoulos, "Stability and phase error analysis of FD-TD in dispersive dielectrics," *IEEE Trans. Antennas Propagat.*, vol. 42, pp. 62–69, 1994.

[11] C. A. Balanis, C. A., *Advanced Engineering Electromagnetics.* New York: Wiley, 1989.

[12] A. Taflove and K. R. Umashankar, "The finite-difference time-domain method for numerical modeling of electromagnetic wave interactions," *Electromagnetics*, vol. 10, pp. 105–126, 1990.

[13] A. Taflove and M. E. Brodwin, "Numerical solution of steady-state electromagnetic scattering problems using the time-dependent Maxwell's equations," *IEEE Trans. Microwave Theory Tech.*, vol. 23, pp. 623–630, 1975.

[14] P. G. Petropoulos, "Phase error control for FD-TD methods of second and fourth order accuracy," *IEEE Trans. Antennas Propagat.*, vol. 42, pp. 859–862, 1994.

[15] W. C. Chew, *Waves and Fields in Inhomogeneous Media.* New York: Van Nostrand, 1990.

[16] K. S. Kunz and R. J. Luebbers, *The Finite Difference Time Domain Method for Electromagnetics.* Boca Raton, FL: CRC, 1993.

[17] J. R. Wait, *Electromagnetic Wave Theory.* New York: Harper & Row, 1985.

Jeffrey L. Young (S'89–M'89), photograph and biography not available at the time of publication.

Amorn Kittichartphayak was born on May 2, 1971 in Bangkok, Thailand. He received the B.S. degree in electrical engineering from the University of Idaho, Moscow. Currently, he is a Research Assistant at the University of Idaho working towards his M.S. degree in electrical engineering.

His area of interest is in computational electromagnetics, with emphasis in FDTD methods.

Yuk Ming Kwok received the B.S. degree in electrical engineering from the University of Idaho, Moscow in 1994. Currently, he is a Research Assistant at the University of Michigan working towards his M.S. degree in electrical engineering.

His current research interest is in applied optics.

Dennis Sullivan received the Ph.D. degree from the University of Utah in 1987.

From 1987 to 1993, he was a Research Engineer at the Stanford Medical Center, primarily development of computer simulation for hyperthermia cancer therapy. He is presently an Assistant Professor of electrical engineering at the University of Idaho. His research interest is computer simulation of electromagnetics, particularly in the field of nonlinear optics.